Supporting Information

An Ultrafast Supercapacitor Based on 3D Ordered Porous Graphene Film with AC Line Filtering Performance

Jiangli Xue,[†] Zhaoshun Gao,*,[†] Liye Xiao,[†] Tingting Zuo,[†] Jian Gao,[‡] Dawei Li[†] and Liangti Qu*,[‡]

[†] Interdisciplinary Research Center, Institute of Electrical Engineering, Chinese Academy of Sciences, Beijing 100190, P. R. China.

[‡] Key Laboratory of Cluster Science, Ministry of Education of China; Beijing Key Laboratory of Photoelectronic/Electrophotonic Conversion Materials; School of Chemistry, Beijing Institute of Technology, Beijing 100081, P. R. China.

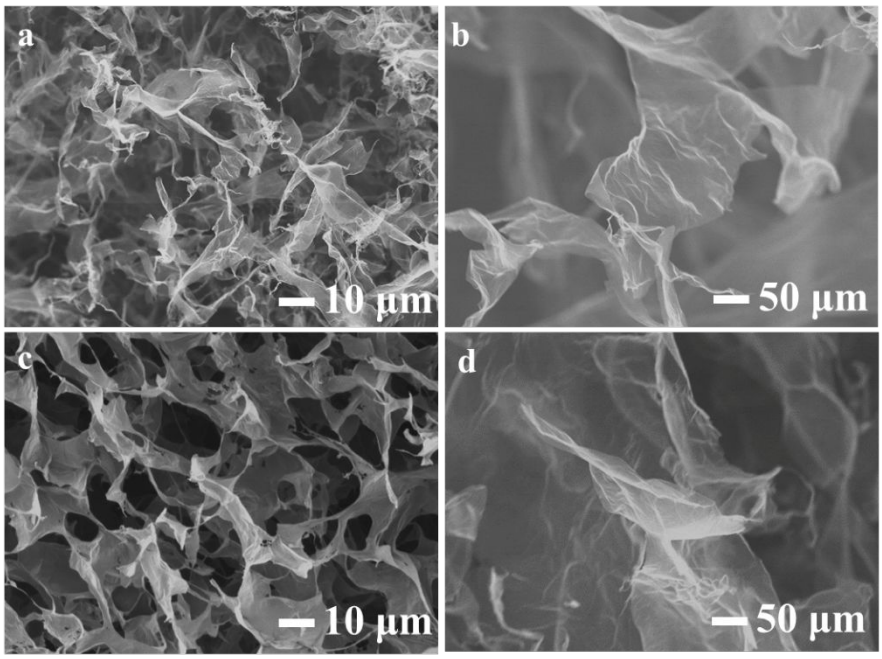

Figure S1. a, b) SEM images of rGO foam with the concentration of 1 mg mL^{-1}. c, d) SEM images of conventional rGO foam with concentration of 3 mg mL^{-1}.

The relatively thin and small sheets of graphene were obtained by using the low concentration of GO suspension due to the solvent prompting diffusion of graphene sheets. The corresponding big sheets were obtained by using conventional concentration of graphene suspension. It is obviously to see that the graphene sheets were smaller and thinner through freeze drying by low concentration of GO suspension (Figure S1a, b) than by comparatively high concentration of GO suspension (Figure S1c, d).

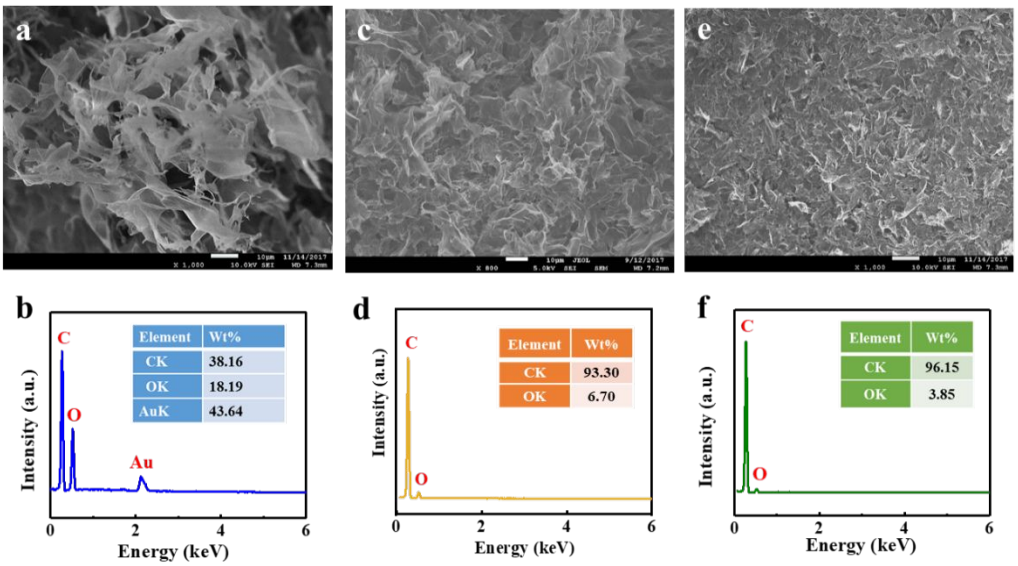

Figure S2. a, c, e) Typical SEM image of the GO foam obtained by freeze drying GO suspension (a), rGO foam with high concentrate (3 mg/mL) obtained by annealing (c) and O-PGF obtained through RS strategy (e). b, d, f) EDS of the GO foam (b), rGO foam (d) and O-PGF (f). The tables inset in (b), (d) and (f) are the corresponding quantitative elemental analysis results.

It's obviously to find that there are only two elements (C and O) for the three samples (Au comes from gold sputtering in GO foam). The GO foam with C/O ratio of 2.10, and the rGO foam with C/O ratio of 13.92, while the O-PGF with a high C/O ratio of 24.97, which demonstrates that the O-PGF reduced more completely by high temperature reducing with low concentrate GO for freeze drying.

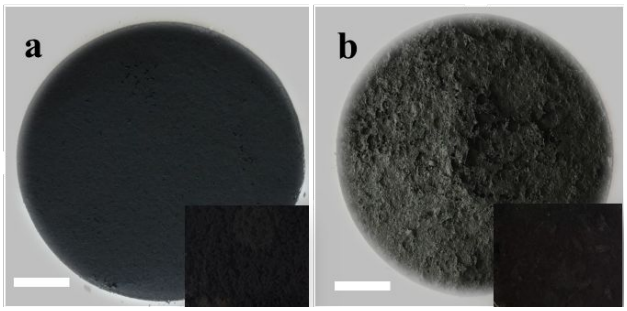

Figure S3. a, b) Digital photograph of O-PGF with different GO concentration. The O-PGF was obtained by vacuum filtering of the rGO suspension with the relative low GO concentration (1 mg mL^{-1}) (a) and with the conventional GO concentration (3 mg mL^{-1}). The photos inset in (a) and (b) are the corresponding state of rGO suspension, respectively. The scale bar is 5 cm.

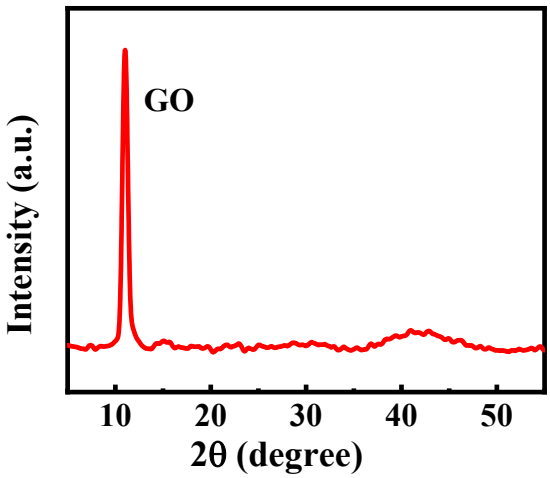

Figure S4. XRD were used to characterize the GO foam. XRD pattern shows the representative peak of 11.02° of GO.

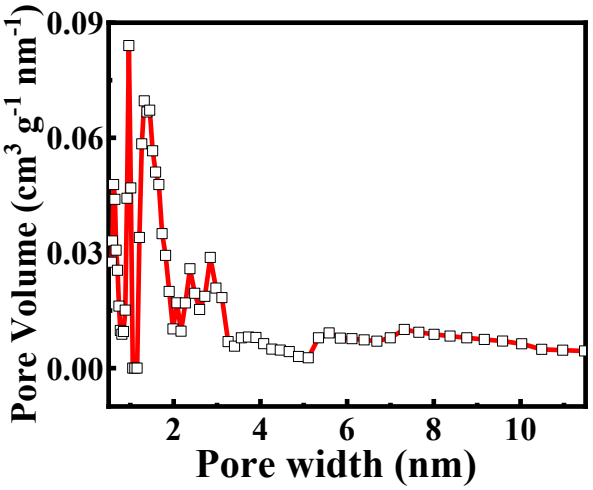

Figure S5. The corresponding pore-size distribution (PSD) curve of O-PGF obtained by using Barrett-Joyner-Halenda (BJH) method.

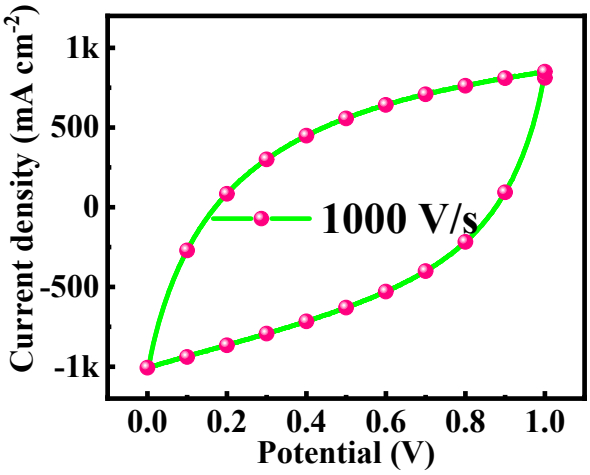

Figure S6. CV curve of the O-PGF based ECs obtained at scan rate of 1000 V s^{-1}.

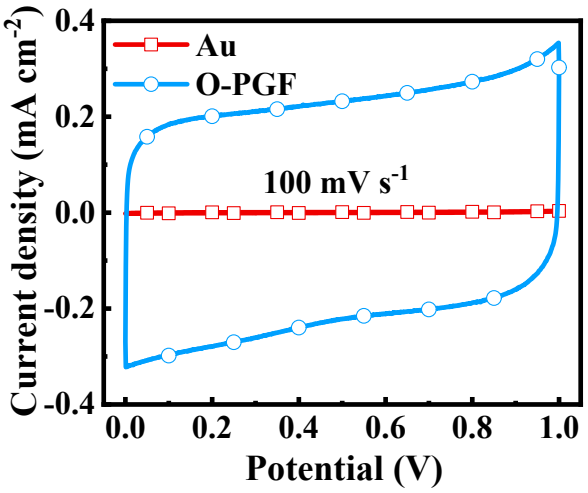

Figure S7. CV curves of the O-PGF based ECs in comparison with the capacitor using gold foil as electrodes, in which gold foils replace the O-PGF electrodes.

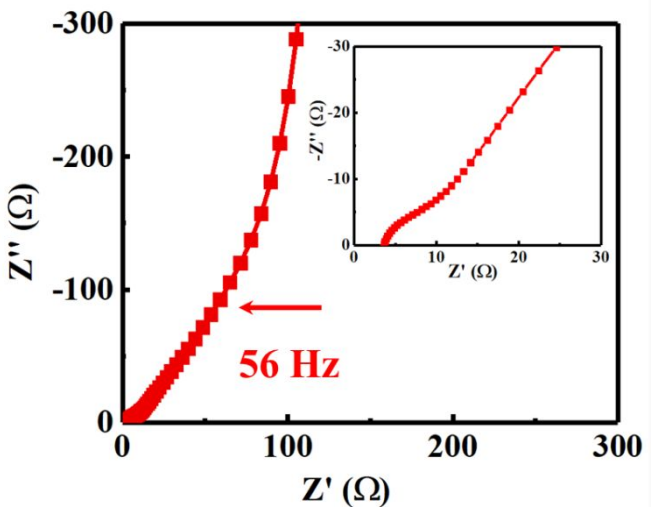

Figure S8. Nyquist plot; inset: the expanded view at high frequencies.

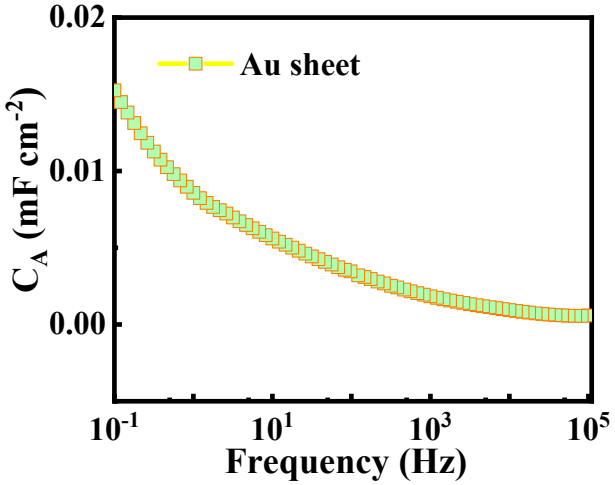

Figure S9. Plot of specific areal capacitance (C_A) as a function of frequency for ECs with bare gold electrodes.

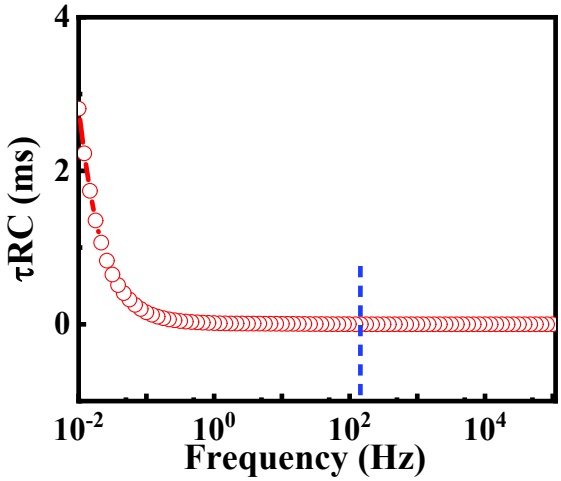

Figure S10. Plot of τ_{RC} as a function of frequency for O-PGF based ECs. At 120 Hz, the τ_{RC} is 0.98 ms which is much shorter than AECs (8.3 ms).

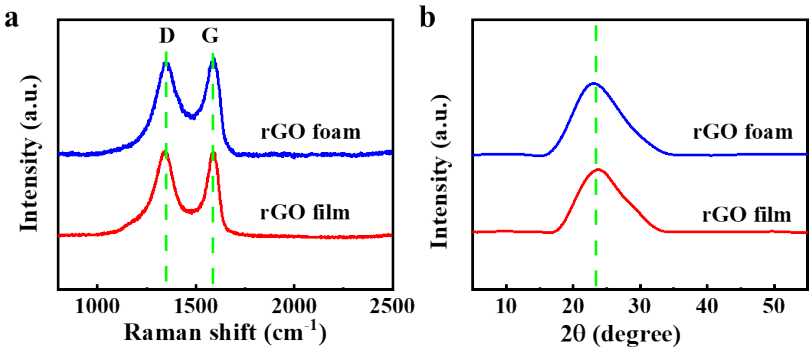

Figure S11. a, b) Raman spectra (a) and XRD patterns (b) of rGO foam and rGO film, respectively.

The Raman spectrum of rGO film exhibits two prominent bands at around 1350 and 1591 cm^{-1}, which are attributable to the D and G bands of thermally reduced graphene oxide (Figure S7a). No shift in the D or G band is observed for rGO foam and even for O-PGF (Figure 2h), which indicates these samples with the same chemical construction. This was also verified by the corresponding XRD patterns with similar diffraction peaks at $2\theta \approx 23.7°$ (Figure S7b).

Table S1. Summary of the other similar work in recent years from the literature and this article.

Materials	Phase at 120 Hz	τ_{RC} (ms)	τ_o (ms)	RC (V/s)	C_S (mF/cm^2)	C_A (mF/cm^2)	Refence
AEC	85.5°	8.3		N/A	N/A	N/A	commercial
G	82	0.2	N/A	N/A	N/A	0.175	s1
ErGO	84	1.35	0.238	400	0.487	0.283	s2
TRGO	30	2.3	4.1	0.5	N/A	3.55	s3
CNT film	82.2	0.181	0.501	450	N/A	0.282	s4
VG	75.4	0.35	1.9	8	0.32	N/A	s5
PEDOT-MSC	65	0.8	3.3	500	9	N/A	s6
carbon sponge	78	0.319	0.371	N/A	N/A	0.172	s7
Ultrathin Printable Graphene	55-70	<1	1.0-2.9	2000	1	0.179	s8
[EMM][NTf_2]/SOS (90 μm)	69.4	N/A	2.512	N/A	N/A	0.082	s9
PEDOT:PSS films	83.6	0.15	0.588	1000	N/A	0.994	s10
OMC	80	560	1	450	0.963	0.559	s11
(TEAOH)-Based polymer	81	0.16	0.63	1000	0.119	0.04	s12
PiCBA	73	0.83	0.27	50	0.15	N/A	s13
Ketjen black	80	8.3	N/A	600	1.2	0.574	s14
ERLGO	80.5	0.219	0.563	1000	N/A	0.151	s15
SWCNT film	75.2	0.2	N/A	500	N/A	N/A	s16
GMFs	82.3	0.32	N/A	2000	0.306	N/A	s17
rGO/PEDOT:PSS	81.4	N/A	0.517	500	5365	N/A	s18
1T $MoS_{2x}Se_{2(1-x)}$	63	1.3-3.2	N/A	1000	0.45	N/A	s19
(rGO) fibers	76	0.241	0.68	500	N/A	N/A	s20
EOG	80.5	N/A	0.073	1000	1.07	N/A	s21
(PEDOT) film/ErGO	82	0.067	0.464	2000	N/A	0.27	s22
VOGN	80	1	N/A	1000	0.055	0.038	s23
MSCs	73.2	N/A	0.32	1000	11.6	0.151	s24
O-PGF	**53**	**0.98**	**1.46**	**2000**	**3.8**	**0.755**	**This work**

s1. Miller J R, Outlaw R A, Holloway B C. Graphene double-layer capacitor with ac line-filtering performance. *Science* **2010**, *329*, 1637-1639.

s2. Sheng K, Sun Y, Li C, et al. Ultrahigh-rate supercapacitors based on eletrochemically reduced graphene oxide for ac line-filtering. *Sci. Rep.* **2012**, *2*, 247.

s3. Nathan-Walleser T, Lazar I M, Fabritius M, et al. 3D micro-extrusion of graphene-

based active electrodes: towards high-rate AC line filtering performance electrochemical capacitors. *Adv. Funct. Mater.* **2014**, *24*, 4706-4716.
s4. Yoo Y, Kim S, Kim B, et al. 2.5 V compact supercapacitors based on ultrathin carbon nanotube films for AC line filtering. *J. Mater. Chem. A.* **2015**, *3*, 11801-11806.
s5. Wu Z, Li L, Lin Z, et al. Alternating current line-filter based on electrochemical capacitor utilizing template-patterned graphene. *Sci. Rep.* **2015**, 5, 10983.
s6. Kurra N, Hota M K, Alshareef H N. Conducting polymer micro-supercapacitors for flexible energy storage and Ac line-filtering. *Nano Energy* **2015**, 13, 500-508.
s7. Joseph J, Paravannoor A, Nair S V, et al. Supercapacitors based on camphor-derived meso/macroporous carbon sponge electrodes with ultrafast frequency response for ac line-filtering. *J. Mater. Chem. A.* **2015**, 3, 14105-14108.
s8. Wu Z S, Liu Z, Parvez K, et al. Ultrathin printable graphene supercapacitors with AC line-filtering performance. *Adv. Mater.* **2015**, 27, 3669-3675.
s9. Kang Y J, Yoo Y, Kim W. 3-V solid-state flexible supercapacitors with ionic-liquid-based polymer gel electrolyte for AC line filtering. *ACS Appl. Mater. Interfaces* **2016**, 8, 13909-13917.
s10. Zhang M, Zhou Q, Chen J, et al. An ultrahigh-rate electrochemical capacitor based on solution-processed highly conductive PEDOT: PSS films for AC line-filtering. *Energy & Environ. Sci.* **2016**, 9, 2005-2010.
s11. Yoo Y, Kim M S, Kim J K, et al. Fast-response supercapacitors with graphitic ordered mesoporous carbons and carbon nanotubes for AC line filtering. *J. Mater. Chem. A.* **2016**, 4, 5062-5068.
s12. Gao H, Li J, Miller J R, et al. Solid-state electric double layer capacitors for ac line-filtering. *Energy Storage Mater.* **2016**, 4, 66-70.
s13. Yang C, Schellhammer K S, Ortmann F, et al. Coordination polymer framework based on-chip micro-supercapacitors with AC line-filtering performance. *Angew. Chem. Int. Ed. Engl.* **2017**, 56, 3920-3924.
s14. Yoo Y, Park J, Kim M S, et al. Development of 2.8 V Ketjen black supercapacitors with high rate capabilities for AC line filtering. *J. Power Sources* **2017**, 360, 383-390.
s15. Chi F, Li C, Zhou Q, et al. Graphene-based organic electrochemical capacitors for AC line filtering. *Adv. Energy Mater.* **2017**, 7, 1700591.
s16. Chen C, Cao J, Wang X, et al. Highly stretchable integrated system for micro-supercapacitor with AC line filtering and UV detector. *Nano Energy* **2017**, 42, 187-194.
s17. Zhang Z, Liu M, Tian X, et al. Scalable fabrication of ultrathin free-standing graphene nanomesh films for flexible ultrafast electrochemical capacitors with AC line-filtering performance. *Nano energy* **2018**, 50, 182-191.
s18. Zhang M, Yu X, Ma H, et al. Robust graphene composite films for multifunctional electrochemical capacitors with an ultrawide range of areal mass loading toward high-rate frequency response and ultrahigh specific capacitance. *Energy & Environ. Sci.* **2018**, 11, 559-565.
s19. Sellam A, Jenjeti R N, Sampath S. Ultrahigh-rate supercapacitors based on 2-

dimensional, 1T $MoS_{2\,x}\,Se_{2\,(1-x)}$ for AC line-filtering applications. *J. Phys. Chem. C* **2018**, 122, 14186-14194.

s20. Gao K, Wang S, Liu W, et al. All fiber based electrochemical capacitor towards wearable AC line filters with outstanding rate capability. *Chem. Electro. Chem.* **2019**, 6, 1450-1457.

s21. Islam N, Hoque M N F, Li W, et al. Vertically edge-oriented graphene on plasma pyrolyzed cellulose fibers and demonstration of kilohertz high-frequency filtering electrical double layer capacitors. *Carbon* **2019**, 141, 523-530.

s22. Wu M, Chi F, Geng H, et al. Arbitrary waveform AC line filtering applicable to hundreds of volts based on aqueous electrochemical capacitors. *Nat. Commun.* **2019**, 10, 1-9.

s23. Li J, Gao H, Miller J R, et al. Study of solid alkaline electrolyte under high temperatures and its application in electrochemical capacitors for AC line-filtering. *J. Power Sources* **2019**, 417, 145-149.

s24. Zhao D, Chang W, Lu C, et al. Charge transfer salt and graphene heterostructure-based micro-supercapacitors with alternating current line-filtering performance. *Small* **2019**, 1901494.